A Data-Driven Approach to Estimating Capacitor Degradation in Reactor Protection Systems

Hye Seon Jo, Ho Jun Lee, Dong Geon Jang, Jin Seong Kim, Man Gyun Na*
Department of Nuclear Engr., Chosun Univ., 10, Chosundae 1-gil, Dong-gu, Gwangju, 61452
**Corresponding author: magyna@chosun.ac.kr*

Keywords: capacitor, remaining useful life, reactor protection system

1. Introduction

Reactor Protection System (RPS), which is a safety-class control system in nuclear power plants, consists of various electronic components and control cards. RPS generates a signal of initiating a reactor trip when necessary under abnormal conditions; thus, any malfunction may have a significant impact on plant safety. Therefore, early detection of potential faults or performance degradation is important, and the development of technologies that can proactively predict failures during plant operation is required. Accordingly, research on condition diagnosis and failure prediction is currently being conducted on electronic components within RPS.

In previous studies [1-3], condition diagnosis and Remaining Useful Life (RUL) prediction models were developed for photocouplers in RPS. This study aims to predict the RUL of capacitors among the electronic components included in RPS. Capacitors are included in power modules and are components that provide stable power by storing and discharging electrical energy. To develop an RUL prediction model for capacitors, data acquired through charge-discharge tests at high temperatures were utilized. Based on these data, the degradation characteristics of the capacitors were analyzed. Furthermore, the Arrhenius equation was employed to convert the accelerated aging data to actual operating temperature conditions and to generate temperature variation datasets. Additionally, a Long Short-Term Memory (LSTM)-based approach, consistent with previous studies [2, 3], was applied to develop the RUL prediction model. The applicability of this approach to the capacitor dataset was assessed through performance comparisons with other approaches.

2. Methods

2.1 LSTM-Based RUL Prediction with Uncertainty Quantification

LSTM models have been widely adopted in studies on RUL prediction, and they have also been extensively applied in time-series forecasting tasks. In this study, we employed a method combining LSTM and Monte Carlo (MC) dropout technology, which has been used in previous studies [2, 3]. This approach demonstrated superior prediction performance for photocouplers in previous studies, and it was applied in this study to assess its applicability. LSTM with MC dropout generates multiple prediction results for the same input data based on the specified number of iterations. In this process, different prediction results were generated, and the mean and standard deviation were used to derive the final prediction value and its associated uncertainty. Fig. 1 shows the structure of the LSTM with MC dropout used in this study. The model is composed of LSTM and dropout layers, and dropout was applied during both training and testing stages to enable uncertainty quantification. The model was developed based on hyperparameter optimization results obtained in previous studies [2, 3]. In addition, the number of iterations used to obtain the prediction results were set to 100.

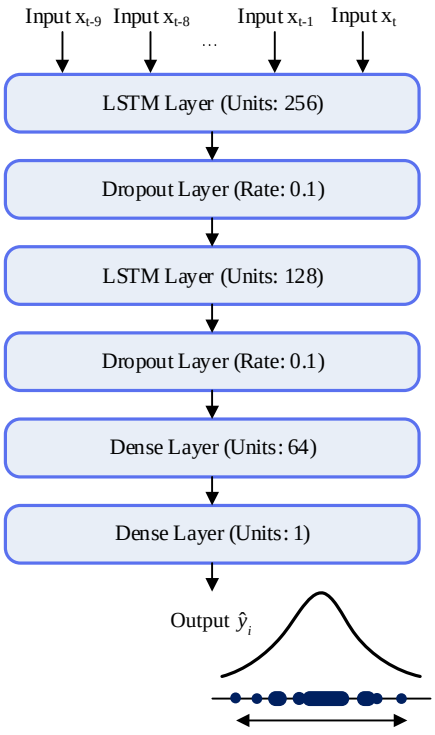

Fig. 1. Structure of the LSTM with MC dropout.

2.2 Physics-Informed Loss Function

In developing the model based on the structure of the LSTM with MC dropout model described above, a loss function was designed that considered both prediction

errors and physics-based constraints. Eq. (1) represents the loss function, which consists of three terms corresponding to the error minimization term, the monotonic decrease constraint, and the boundary condition. The first term corresponds to error minimization, which is commonly used in prediction problems, and was designed to reduce the difference between the real and predicted values. To ensure efficient maintenance, the loss function was formulated to assign an additional penalty to cases where the predicted RUL is greater than the real RUL, thereby penalizing the prediction of delayed failure time. The monotonic decrease and boundary condition terms were introduced to incorporate the inherent properties of RUL, ensuring that the predicted RUL decreases over time and remains non-negative. The model was trained using the proposed loss function, with parameters (α, γ, β) set to balance the contributions of the three terms.

$$E_{Loss} = (1-\alpha)\cdot E_{\min} + \alpha\cdot\gamma\cdot E_{MDC} + \beta\cdot E_{BCC} \qquad (1)$$

where

$$E_{\min} = \begin{cases} \sum_{i=1}^{n} e^{-\left(\frac{\hat{y}_i - y_i}{13}\right)} - 1, & \text{for } \hat{y}_i - y_i < 0 \\ \sum_{i=1}^{n} e^{\left(\frac{\hat{y}_i - y_i}{10}\right)} - 1, & \text{for } \hat{y}_i - y_i \geq 0 \end{cases}$$

$$E_{MDC} = \frac{1}{n-1}\sum_{i=2}^{n}\left[\text{ReLU}(\hat{y}_i - \hat{y}_{i-1})\right]^2$$

$$E_{BCC} = \frac{1}{n}\left\{\sum_{i=1}^{n}\left[\text{ReLU}(-\hat{y}_i)\right]^2 + \sum_{i=1}^{n}\left[\text{ReLU}(\hat{y}_i - 1)\right]^2\right\}$$

α : Parameter to balance error minimization and monotonic decreasing constraints

γ : Parameter to scale the monotonic decreasing constraints

β : Parameter to control boundary condition constraints

$\hat{y}_i$: Predicted value

y_i : Real value

3. Accelerated Aging Data

The capacitors included in the RPS power module serve to ensure a stable power supply. The capacitors were selected as critical components because their performance degradation or failure can affect the functionality of the RPS. Capacitors vary depending on their materials and capacitance values. In this study, an electrolytic capacitor with a capacitance of 330 μF was utilized as the test specimen. Charge-discharge tests were conducted at 130℃ by a collaborating research institute, and the degradation characteristics of the capacitors were analyzed based on the acquired data. The charge-discharge tests were conducted on 40 components, and 1 cycle was defined as 20 minutes of charging and 40 minutes of discharging. Fig. 2 presents voltage profile over 40 minutes, rather than the full one-hour voltage profile. Specifically, 20 minutes of charging and 20 minutes of discharging are shown, while the remaining 20 minutes were intentionally not recorded to clearly distinguish between consecutive cycles.

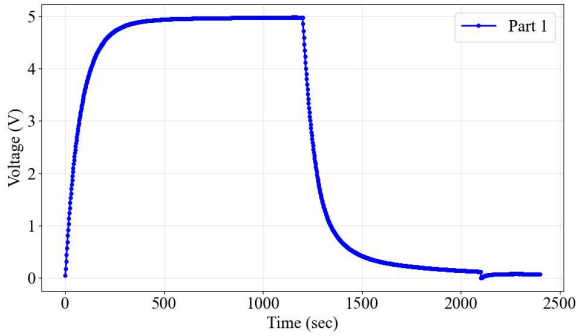

Fig. 2. Voltage profile over one cycle for the first capacitor.

The tests were conducted for approximately 4 months. The capacitors have a degradation characteristic in which their capacitance decreases over repeated cycles, and failure is defined as a 20% reduction in capacitance. Fig. 3 presents the maximum voltage extracted for each channel at each cycle as a box plot, which exhibits a decreasing trend as the number of cycles increases. In addition, the 20th percentile value of the 40 components was adopted as the representative value. In this study, the failure time was defined as the point at which the voltage decreased by 20% compared to the initial voltage (i.e., the voltage at the first cycle).

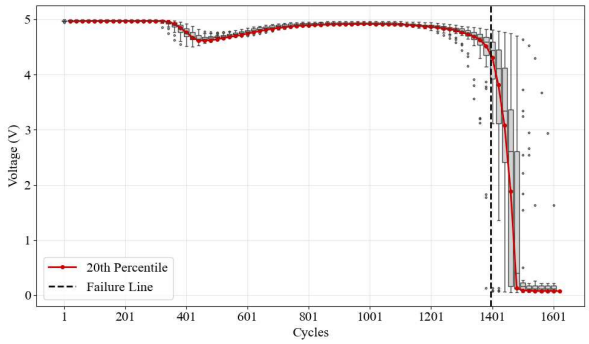

Fig. 3. Maximum voltage per channel depending on number of cycles.

Based on the defined failure point, data were transformed to temperature conditions ranging from 20 to 85℃ using the Arrhenius equation in Eq. (2). Specifically, the acceleration factor at the desired temperature was calculated using Eq. (2), and the 130℃ data were converted to the desired temperature data by multiplying by this factor. In addition, 1,440 temperature variation scenarios were generated considering seasonal effects and temporary heat generation due to faults. The datasets were then created based on these scenarios. The

datasets consist of time-dependent temperature variations and the corresponding changes in RUL based on the average failure rate. Here, the RUL value is calculated by subtracting the current time from the failure time. The transformed and generated data were divided into training, validation, and test datasets and used to develop the RUL prediction model.

$$AF = \exp\left(\frac{E_a}{k}\left(\frac{1}{T_{norm}} - \frac{1}{T_{harsh}}\right)\right) \quad (2)$$

where

E_a : Activation energy ($0.4eV$ [4])

k : Boltzmann constant ($8.617\times10^{-5} eV/K$)

T_{norm} : Temperature under normal conditions (K)

T_{harsh} : Temperature under accelerated conditions (K)

4. Prediction Results

Mean Absolute Error (MAE) and accuracy were adopted as performance metrics to evaluate the prediction model. MAE quantifies the mean absolute difference between the real and predicted values, whereas accuracy is determined by whether the predicted values are within a $\pm10\%$ tolerance range of the real values. Also, environmental variables expected to be obtainable were used as input variables for model development. These included operating time, temperature, the cumulative integral of temperature over time, and the minimum and maximum temperatures.

To assess the applicability of the proposed model, which was developed based on these input variables, its performance was compared with that of other models. For this purpose, a Deep Neural Network (DNN) and an LSTM model were implemented as baseline models. Both models were implemented with MC dropout and were trained using the Mean Squared Error (MSE) loss function. Table I shows the RUL prediction performance among methods. When trained using the MSE loss function, the DNN model exhibited significantly lower prediction performance than the LSTM model. Furthermore, the LSTM model with the proposed Physics-Informed (PI)-loss achieved approximately 2.4% higher accuracy on the test dataset compared to the LSTM model without PI-loss.

This improvement can also be observed in Figs. 4-6, which present the RUL prediction results under constant 46℃ for each model. The DNN model, which exhibited the lowest prediction accuracy, showed a relatively wide uncertainty band and larger prediction errors, whereas the LSTM-based models demonstrated considerably narrower uncertainty bands and smaller errors. This suggests that LSTM-based approaches are more suitable for RUL prediction, considering the characteristics of time-series data. Fig. 7 presents the RUL prediction results of the proposed model under specific temperature variation scenario. The model demonstrates accurate predictions not only under constant temperature conditions but also temperature variation scenarios. These results are consistent with previous studies [2, 3] on photocoupler RUL prediction, further supporting the applicability of the proposed model to capacitors. However, performance improvements are still required under certain dynamic temperature scenarios, indicating the need for further model optimization and different approaches.

Table I: Comparison of RUL prediction performance among methods

Method	Train data		Test data	
	MAE (days)	Accuracy (%)	MAE (days)	Accuracy (%)
DNN (MSE loss)	23.37	63.69	20.93	65.70
LSTM (MSE loss)	6.90	93.93	8.20	94.21
LSTM (PI-loss)	**4.02**	**97.87**	**6.76**	**96.80**

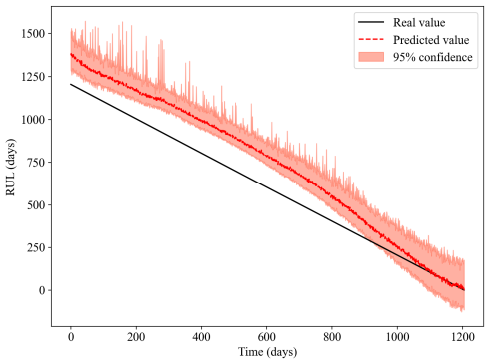

Fig. 4. RUL prediction results of the DNN (MSE loss) model under constant 46℃.

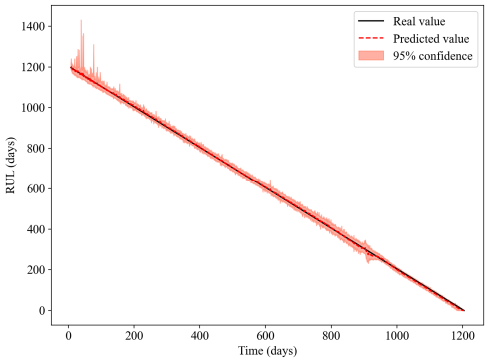

Fig. 5. RUL prediction results of the LSTM (MSE loss) model under constant 46℃.

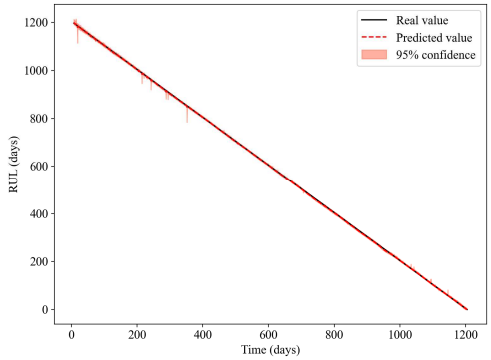

Fig. 6. RUL prediction results of the LSTM (PI-loss) model under constant 46℃.

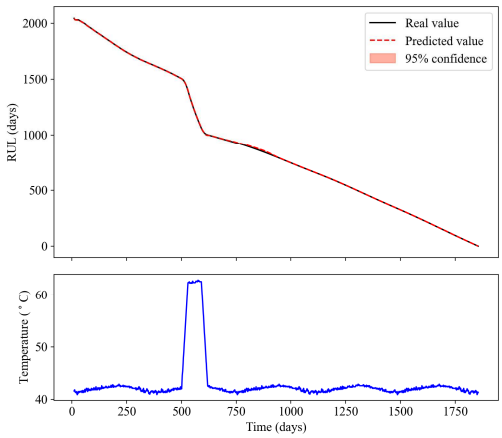

Fig. 7. RUL prediction results of the LSTM (PI-loss) model under specific temperature variation scenario.

5. Conclusions

To prevent potential failures of the RPS and enable efficient maintenance, the RUL prediction model for capacitors was developed in this study as a follow-up to previous studies [2, 3]. To achieve this, charge-discharge test data were obtained under high-temperature conditions. In addition, the degradation characteristics were analyzed, and the failure criteria were defined based on these data. Furthermore, the RUL prediction model was developed using the same data-driven approach as in previous studies [2, 3]. The proposed model achieved 96.8% accuracy in predicting RUL for capacitors, and its applicability was confirmed through performance comparisons with other models. However, further improvements are needed for certain scenarios, and future work should consider model optimization and alternative approaches. While the scope of this study was limited to 330 μF capacitors, experiments on 6800 μF capacitors is currently underway. Consequently, further work is required to develop and extend the model for capacitors with different capacitance and other components.

Acknowledgment

This work was supported by the National Research Foundation of Korea (NRF) grant funded by the Korean Government (MSIT) (No. RS2022-00144239) the Korea Institute of Energy Technology Evaluation and Planning (KETEP) and the Ministry of Climate, Energy & Environment (MCEE) of the Republic of Korea (20224B10100120, Development of commercialization technology for failure diagnosis of reactor control and digital I&C systems).

REFERENCES

[1] H. J. Lee, H. S. Jo, M. G. Na, C. H. Kim, AI-based condition monitoring of photocouplers to enhance the maintenance strategy for digital reactor protection systems, Nuclear Engineering and Technology, Vol.58, No.2, 103958, 2026.
[2] H. S. Jo, H. J. Lee, M. G. Na, C. H. Kim, Deep learning-based RUL prediction with uncertainty quantification for photocouplers in reactor protection systems, Nuclear Engineering and Technology, Vol.58, No.4, 104053, 2026.
[3] H. S. Jo, H. J. Lee, M. G. Na, Failure Prediction of Electronic Components in Reactor Protection System Using LSTM with MC Dropout Technique, Proceedings of the Nuclear Plant Instrumentation and Control & Human-Machine Interface Technology (NPIC&HMIT 2025), June 15-18, 2025, Chicago, IL, US.
[4] J. Torki, C. Joubert, A. Sari, Electrolytic capacitor: Properties and operation, Journal of Energy Storage, Vol.58, 106330, 2023.